


Article

The Study of Graphene Oxide on the Regulations and Controls of the Sol-Gel Film Structure and Its Performance

Yan Gao, Yadong Fan, Junxi Zhang ^{*}, Xuanxuan Liu, Ning Wang and Shengjie Yang

Shanghai Key Laboratory of Material Protection and Advanced Material in Electric Power, Shanghai University of Electric Power, Shanghai 200090, China; yszqbwjhx@mail.shiep.edu.cn (Y.G.); fydyllyjy@163.com (Y.F.); 18311057978@163.com (X.L.); wn15705594854@163.com (N.W.); yangshengjie97@mail.shiep.edu.cn (S.Y.)

* Correspondence: zhangjunxi@shiep.edu.cn

Abstract: A facile strategy to boost anticorrosion potency of graphene oxide/silica hybrid sol-gel coating is developed through fully exploiting the capabilities of graphene oxide (GO). Together with a barrier to corrosives and crack inhibitor, GO was further explored herein as a regulator to regulate the gelation process and provide robust coating films with stratified microstructures and ultimately extended diffusion paths. The sol-gel coating with stratified microstructure achieved on AA5052 aluminum alloy surface afforded greatly enhanced corrosion protection capability as assessed by electrochemical measurements and immersion tests. The corrosion current density of the sample of a hybrid GO sol-gel film was about 30 times less than that of sample of pure sol-gel film sample. The regulation mechanism of GO during the film formation process and the anticorrosive protection properties of the film were discussed.

Keywords: structural regulation; graphene oxide; sol-gel SiO₂ coating; corrosion protection; regulation mechanism



Citation: Gao, Y.; Fan, Y.; Zhang, J.; Liu, X.; Wang, N.; Yang, S. The Study of Graphene Oxide on the Regulations and Controls of the Sol-Gel Film Structure and Its Performance. *Metals* **2022**, *12*, 20. <https://doi.org/10.3390/met12010020>

Academic Editors:
Kamyar Shirvanimoghaddam and
Chang Woo Lee

Received: 15 October 2021
Accepted: 16 December 2021
Published: 22 December 2021

Publisher's Note: MDPI stays neutral with regard to jurisdictional claims in published maps and institutional affiliations.



Copyright: © 2021 by the authors. Licensee MDPI, Basel, Switzerland. This article is an open access article distributed under the terms and conditions of the Creative Commons Attribution (CC BY) license (<https://creativecommons.org/licenses/by/4.0/>).

1. Introduction

Aluminum alloys have the advantages of good installation and transportation [1,2], light weight and high specific strength. They are widely used in aerospace, electrical transmission and transformation architecture [3]. By the complex application environment, the application of aluminum alloy is limited [4].

The organic coating, traditionally used, ages after long service, poor UV resistance and emission of toxic VOC, making it unsuitable for application to outdoor environments. Inorganic coating has good wear resistance, UV resistance and environmental friendliness, which can protect aluminum metal components in power transmission and transformation systems in service [5].

Nowadays, inorganic sol-gel coating is becoming an attractive research field for its environmentally friendly features and low cost [6–8]. Eco-friendly sol-gel coating is second to none as a prospective candidate to substitute traditional conversion coatings [9]. However, large-scale applications of those inorganic coatings are limited by their brittle nature. It is difficult to fabricate crack-free, thick enough sol-gel coating films with sufficient corrosion protection capabilities [10]. Much effort has been devoted to improving their anti-corrosion performance through the introduction of functional additives. For example, organic additives or inhibitors were introduced to upgrade the corrosion protection properties of hybrid films [11]. Functional polyvinyl butyral (PVB) was merged into the sol-gel film to covalently (Si-O-C) bond with the inorganic matrix. The composite film obtained showed improved thickness and was free of cracks [12]. Inorganic metal salt additives, such as Ce(CH₃COO)₃, could bestow hybrid coatings with a self-healing property and enhance their corrosion inhibition ability due to the acceleration of the hydrolysis and condensation processes [13]. Corrosion-resistant inorganic microflakes, such as glass flakes, were also utilized to improve the anti-corrosion property of the sol-gel coatings due to their efficient

barriers against corrosive intrusion and the extended diffusion path of the corrosives. However, the incorporation of nanoparticles and inhibitors sometimes increased the coating instability and reduced the sol-gel film's uniformity due to additive incompatibility and aggregation [14].

With oxygen functional groups (such as -OH, -COOH) on its basal planes and edges, graphene oxide (GO) has been drawing wide attention in coating applications [15]. Moreover, the functional groups of GO provide its good compatibility with the matrices and GO additives. Additionally, GO has a high aspect-ratio flake-like structure and thus has an excellent barrier property [5].

Hence, having splendid physical and chemical properties, graphene oxide (GO) has been extensively explored as an excellent additive to mediate the structures and the properties of coating films [16]. For example, Li et al. [17] reported that when GO was incorporated in poly(vinyl alcohol) (PVA) matrix as an additive, forceful interfacial interactions could be established between the GO and PVA through hydrogen bonding, leading to structural change and improved crystallinity of the PVA/GO nanocomposites. Xue et al. [15] by sol-gel method to make GO modified coating, it was prepared on aluminum alloy. The results demonstrated that GO can be covalently functionalized with silanol from silane coupling agents. The corrosion protective properties of sol-gel film distinctly by providing the good barrier property of layered GO and enhancing the cross-linking density of the film when the concentration of GO is 0.5 mg mL^{-1} .

It is well known that the spherical surfaces of colloid particles can be fabricated smoothly with polymeric coating films through the polymerization of small molecules by taking advantage of the electrostatic interaction [18]. Kang et al. [19] by layer-by-layer (LBL) assembly, the rG-o multilayers were successfully fabricated and transferred to Fe and Cu foils. The results mean that the rG-O layers play a role as a diffusion barrier of gas. The solution process using rG-O was easy and reproducible. Similarly, the surface of colloid microspheres can be homogeneously coated with GO through electrostatic interaction. We envisioned that these properties and techniques could be utilized to renovate the sol-gel coating structure and boost the corrosion protection capabilities of sol-gel composite coating films.

Herein, a feasible strategy to ameliorate the sol-gel coating structure through GO is presented. Shown in Scheme 1a–c are positively charged sol particles, GO, sol-gel/GO film magnified schematic diagram, respectively. The Scheme 1d show the synthesis schematic diagram of sol-gel, positively charged sol particles and negatively charged GO evenly mixed to obtain the coating and both the electrostatic interaction and the bonding between GO and sol are employed to regulate the structure of the coating. Firstly, through adjusting the pH of silica sol particles, which are prepared positively charged silica sol particles. Then the positively charged sol particles is mixed with negatively charged graphene, and the silica sol particles around GO gathers and bonds to GO, forming lamellar structure with similar morphology to GO. In the meantime, the introduction of negatively charged GO also prompts the gelation of the positively charged silica sol to form a stratified structure of hybrid sol-gel/GO film.

In this work, tetraethoxysilane (TEOS) was used as a precursor to prepare the sol solution. Home-made GO was used for the gelation process and incorporated into the sol-gel film. The results showed that the incorporated GO can covalently bond with the sol particles and form a robust heterojunction and also induce the formation of a stratified structure. Electrochemical measurements showed that the resulting sol-gel/GO hybrid achieved through this novel strategy demonstrated a greatly enhanced corrosion protection capability. The regulating mechanism of GO on the gelation process to form the stratified structure is explored in the current research.

first at 60 °C for 80 min, then at 90 °C for 40 min and last at 150 °C for 10 min in the oven, and the obtained sol-gel films were designated as SG film and SG/GO film.

2.3. Characterization Techniques

A scanning electron microscope (SEM, JSM-7800F, JEOL, Tokyo, Japan) was used to observe the surface morphology of the samples. The microstructure of the samples was studied by transmission electron microscopy (HR-TEM, JEM-2100F, JEOL, Tokyo, Japan) equipped with an energy-dispersive X-ray spectrometer (EDX). The TEM samples were peeled from the samples. Raman spectra were performed by exciting a 633 nm wavelength He-Ne laser beam on the sample (confocal Raman), and the power of the laser was set at a minimum (6 mW). The position of the sample to be studied was focused by magnifying the microscope by 50 times. The zeta potential was measured by a Zetasizer Nano (ZS90, Malvern Instruments, Malvern, UK). The Raman spectra were recorded in the wave number range of 1000–2000 cm^{-1} . Electrochemical measurements (electrochemical impedance spectroscopy, polarization curve measurements) were performed with an electrochemical workstation (Interface 1000, Gamry, Philadelphia, PA, USA) in 3.5 wt.% NaCl solution. Polarization curve measurements were tested by sweeping the potential from -0.1 V to 0.1 V (vs. open-circuit potential) at a scan rate of 0.1667 mV/s, and fitted by the fitting tool (nonlinear fitting in a weakly polarized region) provided by the electrochemical workstation. With a sinusoidal perturbation of 5 mV, EIS measurements were conducted at open-circuit potential in the amplitude and a frequency domain from 10^5 Hz to 10^{-2} Hz after 1 h, 72 h, 480 h and 720 h of immersion time. Zview software (V3.3a) was employed to analyze the impedance data. All the potentials were recorded in relation to the saturated calomel electrode (SCE). All tests were performed at room temperature.

3. Results and Discussion

3.1. Chemical Characterization of GO, SG Film and SG/GO Film

The Raman spectra of the GO, SG film and SG/GO film are presented in Figure 1. The Raman spectrum of the SG film has no peak, but two obvious peaks are observed in the spectra of the GO and SG/GO film. Generally, the Raman spectrum of GO exhibits a D band corresponding to defects inherent in the graphite oxide at 1351 cm^{-1} and a G band which is ascribed to the first-order scattering of the E_{2g} vibration mode at 1597 cm^{-1} [22]. The intensity ratio of the D band and G band was 0.935, while that of the SG/GO film was increased to 1.112, which is related to the decrease in size of the in-plane sp^2 area caused by repercussion between sol particles and GO. It is confirmed that a bond is formed between the GO and silica particles [22,23].

3.2. Microstructure of SG Film and SG/GO Film

Figure 2 shows SEM and TEM images of the SG film and SG/GO film. The SG film (as shown in Figure 2a) is smooth from the cross-section and the complete cluster structure does not show any preferential orientation. Based on the SEM image in Figure 2b, a stratified structure with folded edges is formed with the incorporation of GO, and the thickness of the stratified structure is much thicker than that of the graphene oxide layer. Moreover, the SG/GO film exhibits a hierarchical structure characteristic. Figure 2c presents the TEM image of the SG film, which exhibits a uniform gel structure. However, for the SG/GO film (as shown in Figure 2e), stratified structures with uniform dispersion can be observed clearly. The main components in the SG film are silicon and oxygen according to the results of the EDS image (as shown in Figure 2d). Figure 2f corroborates that the observed SG/GO film is composed of GO with the presence of carbon elements.

The differences between the SG film and SG/GO film may be elucidated by the influence of GO on the gelation process of the sol particles owing to its bearing oxygen functional groups on its edges' proximal planes, and negatively charged GO electrostatically attracted positively charged sol particles in solution. From this point of view, the negative electric field generated by GO regulates the polycondensation reaction of the surrounding

sol particles, and controls the local particle alignment, so the sol-gel film finally forms a stratified structure similar to the shape of GO via electrostatic attraction and the bond relationship. This hybrid sol-gel film with a stratified structure is expected to demonstrate excellent corrosion protection performance.

3.3. Corrosion Protection Performance of Bare Al with SG Film and SG/GO Film

The potentiodynamic curves of the bare Al-alloy sample are presented in Figure 3, with SG film and SG/GO film coated specimens after 1 h of immersion in 3.5 wt.% NaCl solution.

Meanwhile, Table 2 lists the fitting results of the derived parameters of the polarization curves. Both the anodic and cathodic responses are significantly influenced by the added GO. The cathodic Tafel slopes ($-\beta_c$) of the SG/GO film show larger values compared to those of the SG film, and the decrease of the cathodic Tafel slopes of the SG/GO film coated samples indicates that the oxygen reduction reaction ($O_2 + 2 H_2O + 4 e \rightarrow 4 OH^-$) on the alloy is effectively reduced by the SG/GO film. It is clearly seen that the anodic Tafel slopes (β_a) of the SG/GO film coated sample are larger than those on the bare Al-alloy sample and SG film coated samples. The results illustrate that the anodic dissolution process ($Al \rightarrow Al^{3+} + 3e$) was weakened for the SG/GO film. In the whole polarization curve, it seems that both the anodic and cathodic current densities of the SG/GO film coated sample drop significantly compared with the SG film coated sample. The corrosion current density (j_{corr}) of the SG/GO film specimen was about 30 times less than that of the SG film coated sample. The incorporation of graphene oxide decreases the corrosion current density from $1.43 \times 10^{-7} A/cm^2$ to $4.62 \times 10^{-9} A/cm^2$. Previous studies attributed these effects to a good barrier property from GO layered [22]. However, for this study, the result may be attributed to the stratified structure controlled by the GO in the coating, which prolongs the diffusion path of the depolarizing agent and aggressive ions. The formation of a stratified structure in the coating inhibits the occurrence and deterioration of corrosion, while increasing the crosslink density of the film to obtain a dense coating. Meanwhile, the stratified structure still maintains its bonding with the sol-gel matrix, which further enhances the compactness of the coating without cracks.

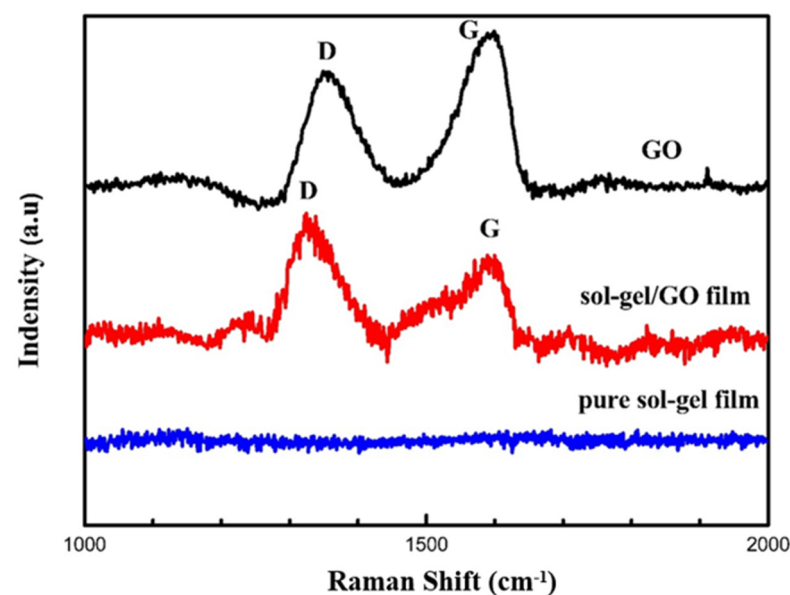


Figure 1. Raman spectra of GO, pure sol-gel film and sol-gel/GO fil.

Table 2. Polarization curve-derived parameters of bare Al sample and samples coated with SG film and SG/GO film.

Simple	E_{corr} (V/SCE)	j_{corr} (10^{-8} A cm^{-2})	ba (V dec^{-1})	$-bc$ (V dec^{-1})
Bare	−0.731	82.4	0.0157	0.128
SG film	−0.749	14.4	0.0511	0.0623
SG/GO film	−0.762	0.463	0.0613	0.0464

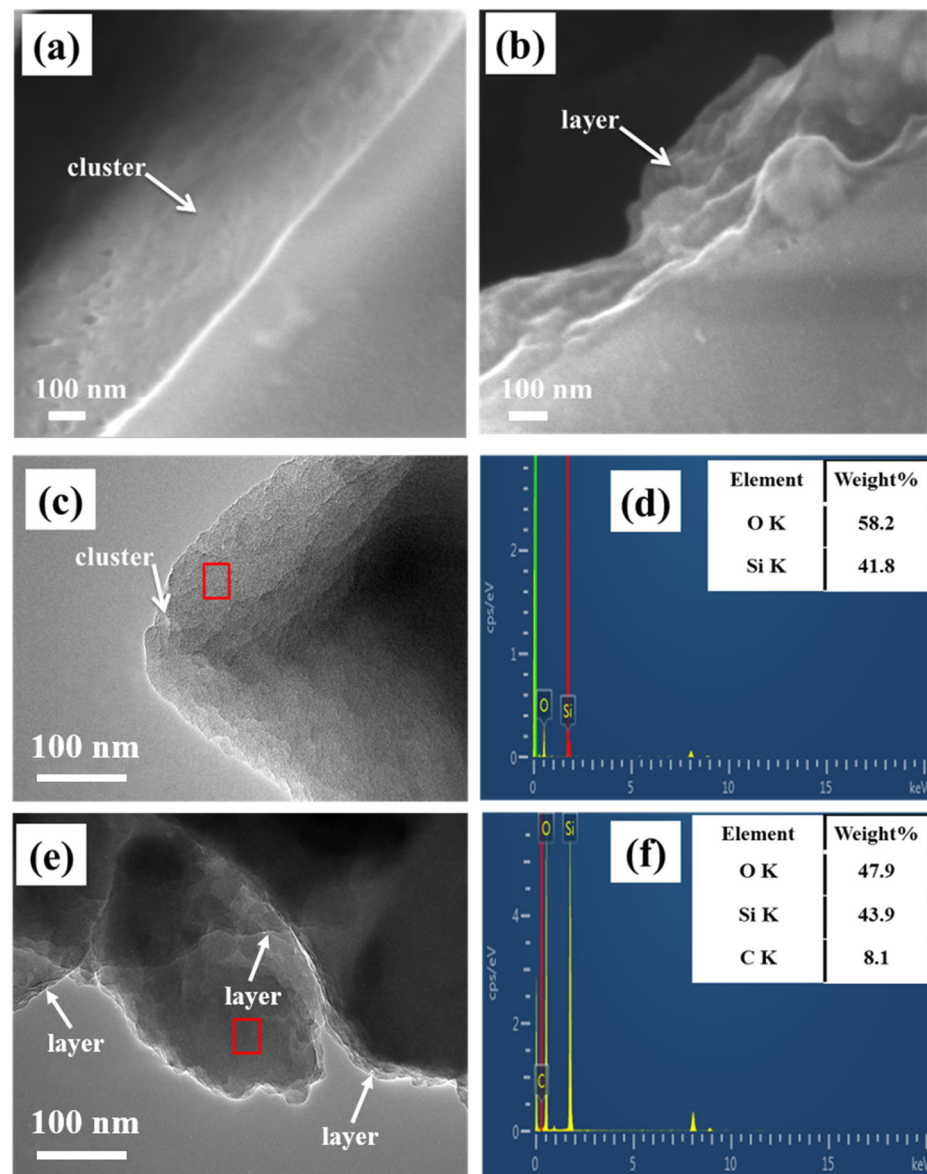
**Figure 2.** (a) SEM image of SG film, (b) SEM image of SG/GO film, (c) TEM image and (d) EDX spectrum of SG film, (e) TEM image and (f) EDX spectrum of SG/GO film.

Figure 4 presents the EIS curves of bare Al-alloy and SG film and SG/GO film coated on AA5052 after 1, 72, 480 and 720 h of immersion in the 3.5 wt.% NaCl solution.

Meanwhile, the surface morphology differed after 1 h, 72 h, 480 h and 720 h. Samples are presented in Figure 5.

The $\log|Z|$ vs. $\log f$ diagram of the SG/GO film and SG film coated samples shows higher impedance modulus values over all the frequency range compared with the bare Al sample. SEM images of the SG film and SG/GO film after a 1 h immersion in 3.5 wt.% NaCl

solution show that the surface of both films still maintains its integrity, and no corrosion is visually observed on the surface (as shown in Figure 5a,e). At the same time, the $|Z|_{0.01\text{Hz}}$ value (about $1.28 \times 10^6 \text{ Ohm cm}^2$) of the SG/GO film coated sample is higher than the value (about $6.79 \times 10^5 \text{ Ohm cm}^2$) of the SG film coated sample. The corrosion protection performance of the sol-gel film was reflected at a low frequency impedance value [24]. In the Bode plots it exhibits three time constant (see Figure 4a,b), which are located in the higher frequency (10^3 – 10^5 Hz), the middle frequency (10^2 – 10^0 Hz) and lower frequency (below 10^{-1} Hz). In the lower frequency it partially overlaps with the peak at the middle frequency, which is related to the intermediate layer and the electrochemical reaction of the matrix [25,26].

After 72 h immersion, the high frequency response peak (10^3 – 10^5 Hz) of the SG film coated sample has almost disappeared from the phase angle spectra (shown in Figure 4d). However, the peak at high frequency of the SG/GO film can still be observed clearly. In terms of the peaks at the middle and low frequency, it is clearly observed that the peak at the low frequency of the SG film and SG/GO film overlap partially with the peak at the middle frequency, and the peaks of the SG/GO film at the middle frequency and low frequency remain the same after 72 h immersion. This means that the substrate is not corroded. Moreover, the films still keep a complete surface according to the surface micrograph obtained (Figure 5f). However, for the SG film, as the immersion time increases, the peak at the middle frequency shows a conversion toward higher frequency. Meanwhile, the peak at low frequency shows a shift to the lower frequencies, indicating that the corrosion protection performance of the SG film is reducing and the substrate is beginning to corrode. Many cracks caused by corrosion products appear on the surface of the SG film (as presented in Figure 5b). With prolonged immersion time, the peak at high frequency shows a continuous decrease after 480 h, the peak at the middle frequency of the SG/GO film shows a shift toward higher frequency and the lower frequency peak shows a shift toward lower frequencies. Figure 5g presents the surface of the sample coated with SG/GO film after 480 h immersion. Peeling of the exfoliated stratified structure occurs on the surface of the substrate, which suggests damage to the SG/GO film. The integrity of the SG/GO film was damaged and the protection performance of the coating reduced. At the same time, the accumulation of corrosion products lead to more cracks on the surface of the SG film (as shown in Figure 5c). After 720 h of immersion (see Figure 4g,h), the peak at high frequency of the SG/GO film coated sample disappears substantially from the spectra. Only the middle and low frequency time constants appeared on the phase angle diagram, which suggests failure of the SG/GO film after 720 h immersion. Visible cracks appear on the surface of the SG/GO film (as shown in Figure 5h). In comparison, for the SG film (as shown in Figure 5d), more severe corrosion emerges on the surface of the SG film coated specimen in contrast with the SG/GO film coated samples. Meanwhile, comparing the surface states of these two coatings, it is easy to see that the destruction processes of the SG film and the SG/GO film are different. Figure 5c shows the SEM image of the SG film after 480 h immersion, from which film delamination and film cracking can be observed. Because the SG film has a rich porosity and brittle nature, the tensile stresses caused by corrosion products cause the SG film to crack. In conclusion, an exfoliated stratified structure can be observed on the SG/GO film (as shown in Figure 5g). The difference between the SG film and SG/GO film is that the stratified structures in the film reduce the damage of the coating by the lateral tensile stress, which avoids cracks in the coating. At the same time, the vertical tensile stress causes the stratified structure to peel from the coating, which damages the SG/GO film. The equivalent electric circuit (EEC) applied for numerical fitting of the EIS data is shown in Figure 6.

By the EEC it is possible to adequately fit the EIS curves of the bare Al sample with a two time constant (as shown in Figure 6a). Meanwhile, the EEC in Figure 6b was applied for the sol-gel coated specimen. The R_{sol} corresponds to the solution resistance. R_{coat} and Q_{coat} were assigned to the resistance and constant phase element relating to the capacitances of the sol-gel, and R_{int} and Q_{int} are related to the resistance and capacitances

of the intermediate layer. The charge transfer resistance and the double layer capacitance seemed to be related with the R_{ct} and Q_{dl} . Figure 6c was applied for the sol-gel film coated sample with the time unaltered in relation to the SG film. The derived parameters are listed in Table 3.

Table 3. Resistances (R_{coat} , R_{int} , R_{ct}) and capacitance (Q_{coat} , Q_{int} , C_{dl}) parameters extracted from EIS data within the test period.

Sample	Time (h)	Q_{coat}		R_{coat} ($\Omega \text{ cm}^2$)	Q_{inter}		R_{inter} ($\Omega \text{ cm}^2$)	C_{dl} ($10^{-6} \Omega^{-1} \text{ cm}^{-2} \text{ s}^n$)	R_{ct} ($\Omega \text{ cm}^2$)	χ^2 (10^{-3})
		Y_0 ($\mu\text{S s}^n \text{ cm}^{-2}$)	n		Y_0 ($\mu\text{S s}^n \text{ cm}^{-2}$)	n				
Bare Al-alloy	1	/	/	/	7.22	0.89	10.8	2.11	2560	5.12
	72	/	/	/	70.1	0.88	7.13	68.1	2500	1.12
	480	/	/	/	890.2	0.83	23.2	84.6	3215	0.71
	720	/	/	/	1356.6	0.80	38.4	89.5	3456	1.56
SG film	1	1.67	0.80	337	5.77	0.83	570,000	5.02	4640	0.42
	72	/	/	/	7.12	0.83	7420.	6.77	5640	0.67
	480	/	/	/	12.5	0.86	84.3	9.52	3841	0.48
	720	/	/	/	16.1	0.83	54.2	12.7	4784	1.23
SG/GO film	1	0.11	0.82	12100	5.33	0.79	1,140,000	4.68	5740	0.24
	72	0.54	0.76	6210	5.19	0.81	714,000	5.93	4210	0.15
	480	0.79	0.73	2149	8.12	0.80	432,000	8.12	3854	0.98
	720	/	/	/	7.06	0.726	1308	3.32	7975	4.30

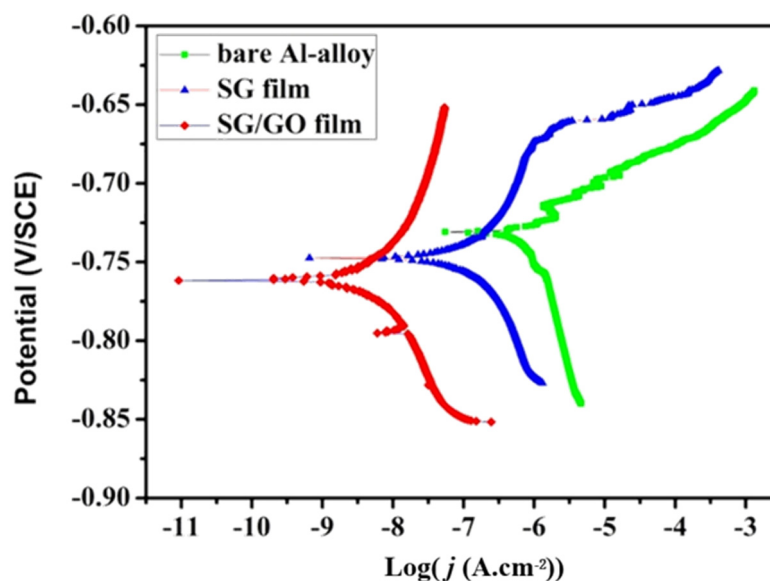


Figure 3. Potentiodynamic polarization curves of bare alloy sample and samples coated with SG film and SG/GO film after 1 h immersion in 3.5 wt.% NaCl solution.

The corrosion protection performance can be evaluated through the value of R_{coat} . At the initial immersion, the R_{coat} value of the SG/GO film is much higher than that of the SG film. The R_{coat} values of the SG film decrease significantly and tend to disappear after immersing for 72 h, indicating that a large number of pores and cracks are formed on the sol-gel layer. In comparison, the R_{coat} of the SG/GO film decreases more slowly with immersion time and remains relatively high even after immersion of 480 h, which indicates the slower formation of cracks in the SG/GO film and the excellent coating barrier performance. The Q_{coat} of the SG film and SG/GO film increases during the immersion tests due to the increase of the dielectric constant for water absorption. Furthermore, the Q_{coat} of the SG/GO film still exhibits a lower value even after a long immersion time. The above analysis indicates that the accretion of GO has a positive influence on the corrosion protection performance of the sol-gel film, which is attributed to the shape of the stratified structure that develops, with a higher cross-link density of the sol-gel film.

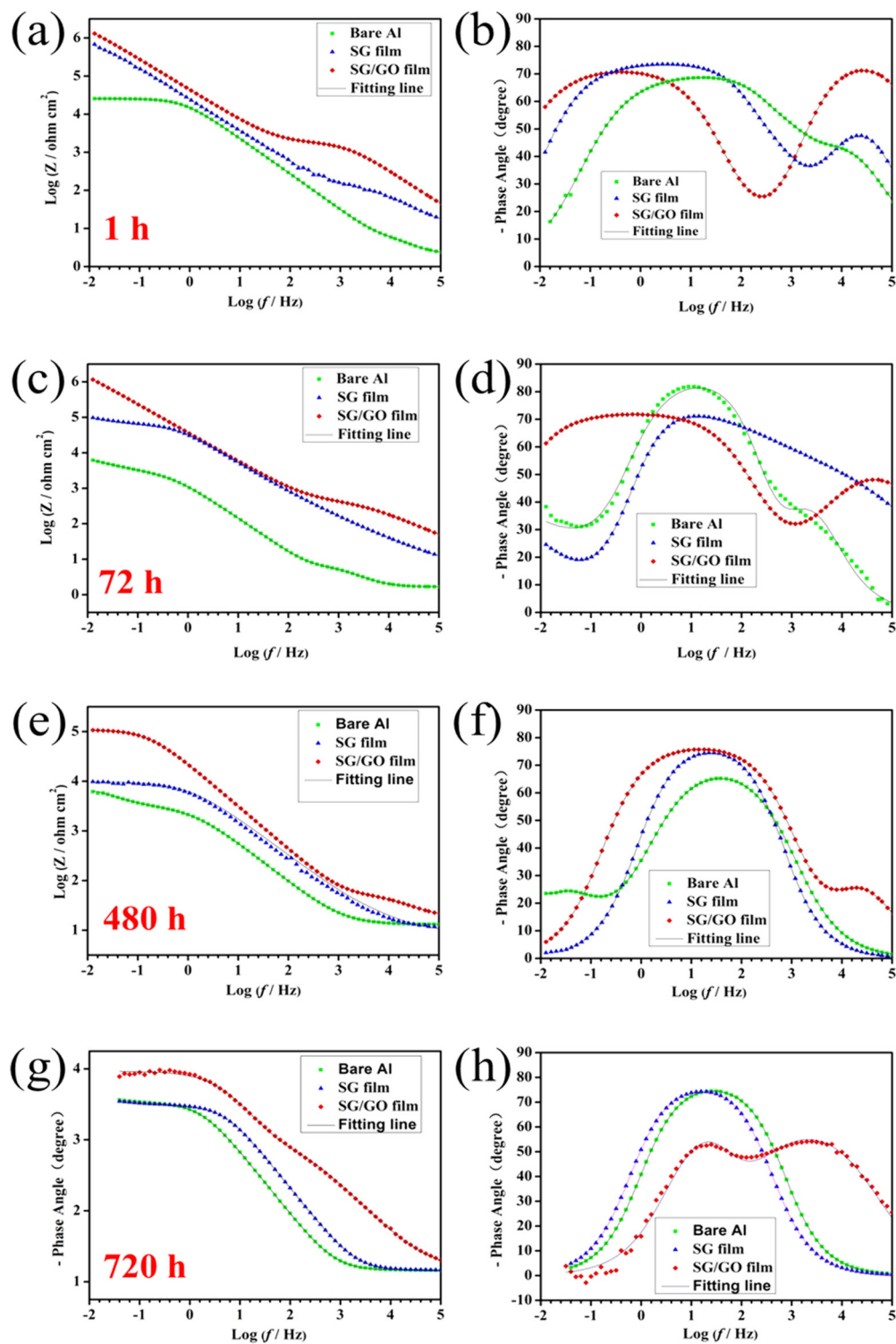


Figure 4. EIS curves and the fitting lines of GO-0 film and GO-1 film coated AA5052 samples after 1, 72, 480 and 720 h of immersion in 3.5 wt.% NaCl solution. (a,b) after 1 h immersion; (c,d) after 72 h immersion; (e,f) after 480 h immersion; (g,h) after 720 h immersion.

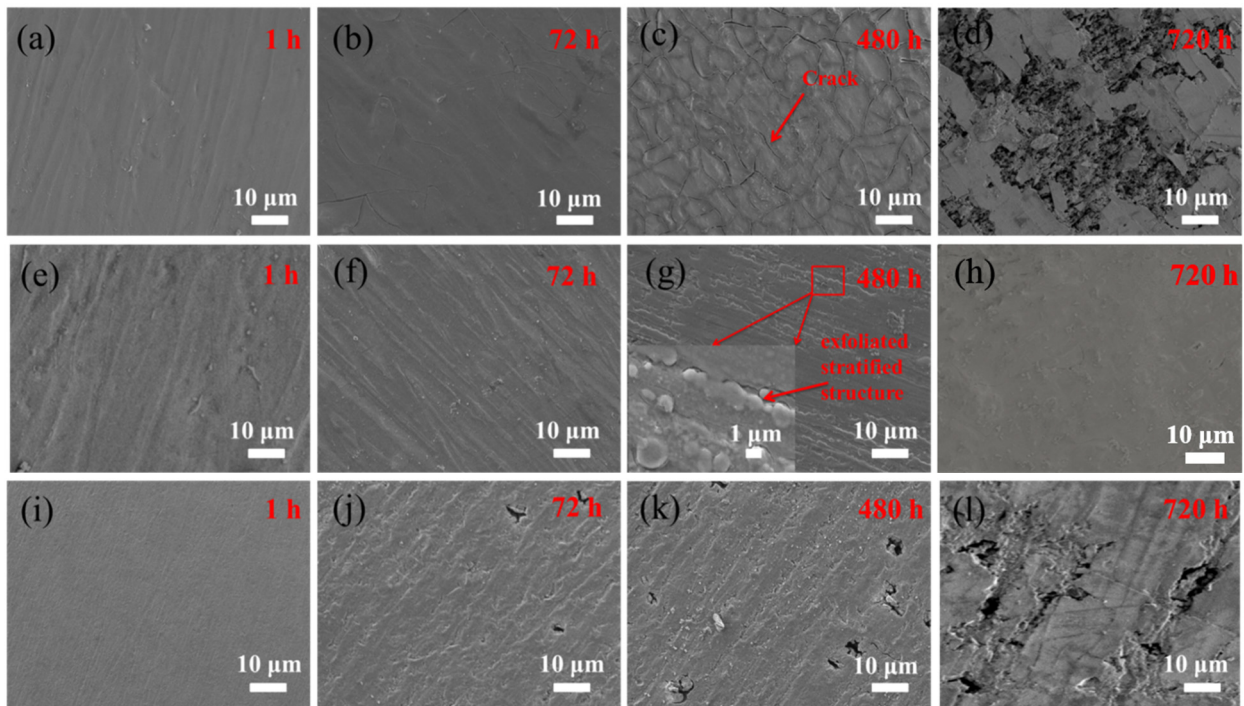


Figure 5. Surface morphology of (a–d) for SG film coated samples and (e–h) for SG/GO film coated samples and (i–l) for bare 5052 Al alloy after 1 h, 72 h, 480 h and 720 h immersion in 3.5 wt.% NaCl solution.

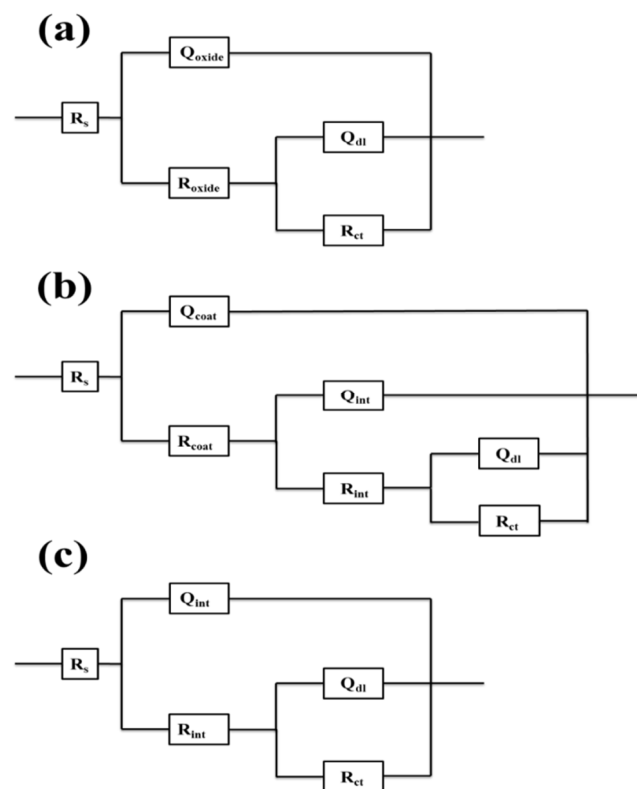


Figure 6. Equivalent electric circuit, (a) bare Al sample, (b) the sol-gel coated sample, (c) the sol-gel film coating failure sample.

The R_{int} value of the SG/GO film is more than that of the SG film after 1 h of soaking. The SG/GO film specimen maintains higher R_{int} values and lower Q_{int} values after 480 h of immersion, which indicates that the intermediate layer still maintains good compactness and integrity. However, the SG/GO film shows a remarkable decrease of the R_{int} value and increase of the Q_{int} value after soaking for 72 h. This suggests the rapid failure of the SG film and the excellent protection properties of the SG/GO film even after successive immersion.

3.4. Coating Formation and Corrosion Protection Mechanism of Samples

Figure 7 shows the schematic illustration of the formation and corrosion protection mechanism of the SG/GO coating.

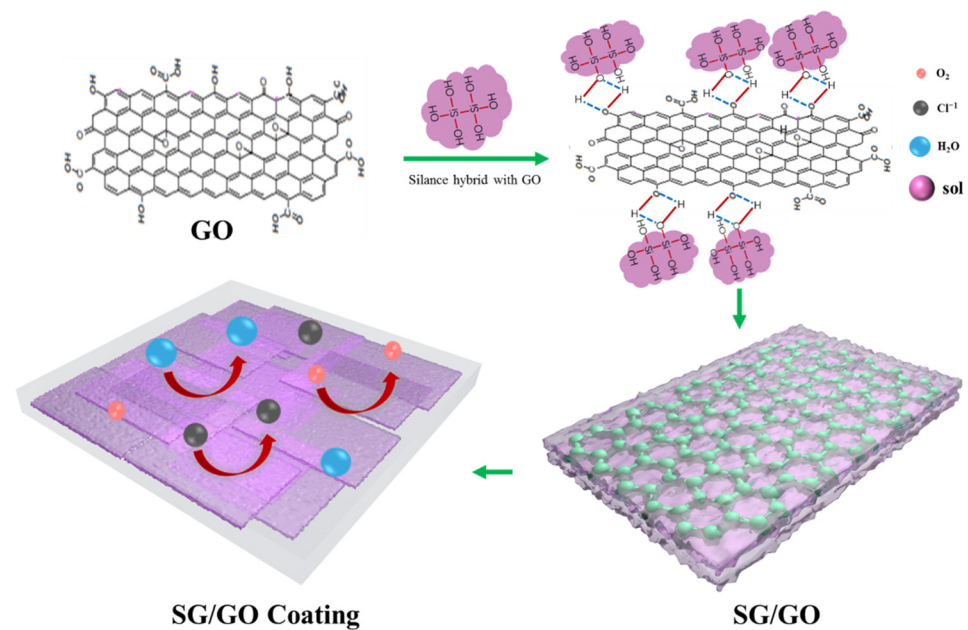


Figure 7. Schematic illustration of formation and corrosion protection mechanism of the coated samples.

The hydroxyl group at the edge of GO lamellar and the π - π bond of GO form p - π conjugated electron cloud [27], hence GO is electronegative as a whole and the Zeta potential of GO was tested to be -6 mV. The zeta potential of silica sol particles was $+5$ mV, which contained Si-OH groups. GO and silica sol were attracted to each other under electrostatic action. Hydroxyl of GO and silica sol were dehydrated and condensed. Silica sol groups are adsorbed by covalent bond around GO and layered SG/GO coating is formed under the guidance of GO. GO could block erosive ions and oxygen reaching the metal matrix [28]. The layered coating improved the crosslinking density and barrier properties, and effectively enhanced the corrosion resistance of SG/GO coating. This conclusion was consistent with our electrochemical test results.

4. Conclusions

Herein, a novel facile strategy was developed to promote the corrosion inhibition property of GO hybrid sol-gel coating (SG/GO film). By taking advantage of the different zeta potentials of GO and sol, GO was exploited as a regulator for the first time to regulate the sol-gel process and produce sol-gel films with a stratified structure. The sol particles are efficiently and densely cross-linked along the GO. Coating films were generated with reduced porosity and enhanced stability. The stratified microstructure inherited from the GO could efficiently extend the diffusion paths of the corrosives and thus improve the corrosion protection performance. Compared with traditional organic coatings, inorganic

coatings had excellent weather resistance and environmental friendliness. After the introduction of GO, the advantages of inorganic coatings such as acid resistance and high salt resistance were increased. These advantages play an important role in metal protection, making the application range of metal wider and effectively improving economic benefits.

Author Contributions: Data curation, Writing—Original draft, Y.G.; Conceptualization, Methodology, Y.F.; Supervision, J.Z.; Investigation, X.L.; Review, N.W.; Visualization, S.Y. All authors have read and agreed to the published version of the manuscript.

Funding: This work was supported by the National Natural Science Funds of China (No. 52171074). This work was also supported by Science and Technology Commission of Shanghai Municipality (No. 19DZ2271100).

Institutional Review Board Statement: Not applicable.

Informed Consent Statement: Not applicable.

Data Availability Statement: The data that support the findings of this study are available from the corresponding author upon reasonable request.

Acknowledgments: The authors highlight their appreciation and gratitude for the availability of and fruitful discussions with our colleagues.

Conflicts of Interest: The authors declare no competing financial interest.

References

1. Mo, Q.; Qin, G.; Ling, K.; Lv, X.; Wang, N.; Li, W. Layer-by-layer self-assembled polyurea layers onto MAO surface for enhancing corrosion protection to aluminum alloy 6063. *Surf. Coat. Technol.* **2021**, *405*, 126653. [[CrossRef](#)]
2. Li, T.; Li, L.; Qi, J.; Chen, F. Corrosion protection of Ti6Al4V by a composite coating with a plasma electrolytic oxidation layer and sol-gel layer filled with graphene oxide. *Prog. Org. Coat.* **2020**, *144*, 105632. [[CrossRef](#)]
3. Ji, L. Study on Corrosion Resistance of Anodized 6463 Aluminum Alloy as Construction Material in 3.5% Sodium Chloride Solution. *Int. J. Electrochem. Sci.* **2021**, *16*, 2. [[CrossRef](#)]
4. Li, J.; Cao, Y.; Wang, Q.; Shang, W.; Peng, N.; Jiang, J.; Liang, L.; Wen, Y. Construction of anodizing/silane/graphene oxide composite film and its corrosion resistance mechanism on aluminum alloy surface. *Mater. Today Commun.* **2021**, *29*, 102999. [[CrossRef](#)]
5. Razavi, S.M.R.; Masoomi, M.; Bagheri, R. Facile strategy toward developing a scalable, environmental friendly and self-cleaning superhydrophobic surface. *Colloids Surf. A Physicochem. Eng. Asp.* **2018**, *541*, 108–116. [[CrossRef](#)]
6. del Olmo, R.; Tiringier, U.; Milošev, I.; Visser, P.; Arrabal, R.; Matykina, E.; Mol, J.M.C. Hybrid sol-gel coatings applied on anodized AA2024-T3 for active corrosion protection. *Surf. Coat. Technol.* **2021**, *419*, 127251. [[CrossRef](#)]
7. Catauro, M.; Tranquillo, E.; Poggetto, G.D.; Naviglio, S.; Barrino, F. Antibacterial Properties of Sol-Gel Biomaterials with Different Percentages of PEG or PCL. *Macromol Symp.* **2020**, *389*, 1900056. [[CrossRef](#)]
8. Catauro, M.; Barrino, F.; Blanco, I.; Piccolella, S.; Pacifico, S. Use of the Sol-Gel Method for the Preparation of Coatings of Titanium Substrates with Hydroxyapatite for Biomedical Application. *Coatings* **2020**, *10*, 203. [[CrossRef](#)]
9. Kaliyannan, G.V.; Palanisamy, S.V.; Priyanka, E.B.; Thangavel, S.; Sivaraj, S.; Rathanasamy, R. Investigation on sol-gel based coatings application in energy sector—A review. *Mater. Today Proc.* **2020**, *45*, 1138–1143. [[CrossRef](#)]
10. Lakshmi, R.V.; Sampath, S.; Aruna, S.T. Silica-alumina based sol-gel coating containing cerium oxide nanofibers as a potent alternative to conversion coating for AA2024 alloy. *Surf. Coat. Technol.* **2021**, *411*, 127007. [[CrossRef](#)]
11. Yu, F.; Akid, R. Corrosion protection of AA2024-T3 alloy by modified hybrid titania-containing sol-gel coatings. *Prog. Org. Coat.* **2017**, *102*, 120–129. [[CrossRef](#)]
12. Ono, S.; Tsuge, H.; Nishi, Y.; Hirano, S.I. Improvement of Corrosion Resistance of Metals by an Environmentally Friendly Silica Coating Method. *J. Sol-Gel Sci. Techn.* **2004**, *29*, 147–153. [[CrossRef](#)]
13. Yu, M.; Liu, Y.; Liu, J.; Li, S.; Xue, B.; Zhang, Y.; Yin, X. Effects of cerium salts on corrosion behaviors of Si-Zr hybrid sol-gel coatings. *Chin. J. Aeronaut.* **2015**, *28*, 600–608. [[CrossRef](#)]
14. Amiri, S.; Rahimi, A. Hybrid nanocomposite coating by sol-gel method: A review. *Iran. Polym. J.* **2016**, *25*, 559–577. [[CrossRef](#)]
15. Xue, B.; Yu, M.; Liu, J.; Liu, J.; Li, S.; Xiong, L. Corrosion protection of AA2024-T3 by sol-gel film modified with graphene oxide. *J. Alloys Compd.* **2017**, *725*, 84–95. [[CrossRef](#)]
16. Zhang, R.; Yu, X.; Yang, Q.; Cui, G.; Li, Z. The role of graphene in anti-corrosion coatings: A review. *Constr. Build. Mater.* **2021**, *294*, 123613. [[CrossRef](#)]
17. Yang, X.; Li, L.; Shang, S.; Tao, X.-m. Synthesis and characterization of layer-aligned poly(vinyl alcohol)/graphene nanocomposites. *Polymer* **2010**, *51*, 3431–3435. [[CrossRef](#)]

18. Yoshinaga, K.; Yokoyama, T.; Sugawa, Y.; Karakawa, H.; Enomoto, N.; Nishida, H.; Komatsu, M. Preparation of monodispersed polymer-modified silica particles by radical polymerization using silica colloid and introduction of functional groups on the composite surface. *Polym. Bull.* **1992**, *28*, 663–668. [[CrossRef](#)]
19. Kang, D.; Kwon, J.Y.; Cho, H.; Sim, J.H.; Hwang, H.S. Oxidation resistance of iron and copper foils coated with reduced graphene oxide multilayers. *ACS Nano* **2012**, *6*, 7763–7769. [[CrossRef](#)]
20. Wang, Q.; Li, X.; Shi, B.; Wu, Y. Experimental and Numerical Studies on Preparation of Thin AZ31B/AA5052 Composite Plates Using Improved Explosive Welding Technique. *Metals* **2020**, *10*, 1023. [[CrossRef](#)]
21. Hummer, W.S.; Offeman, R.E. Functionalized graphene and graphene oxide: Materials synthesis and electronic applications. *J. Am. Chem. Soc.* **1958**, *80*, 1339.
22. Tang, L.-C.; Wan, Y.-J.; Yan, D.; Pei, Y.-B.; Zhao, L.; Li, Y.-B.; Wu, L.-B.; Jiang, J.-X.; Lai, G.-Q. The effect of graphene dispersion on the mechanical properties of graphene/epoxy composites. *Carbon* **2013**, *60*, 16–27. [[CrossRef](#)]
23. Wan, Y.-J.; Gong, L.-X.; Tang, L.-C.; Wu, L.-B.; Jiang, J.-X. Mechanical properties of epoxy composites filled with silane-functionalized graphene oxide. *Compos. Part A Appl. Sci. Manuf.* **2014**, *64*, 79–89. [[CrossRef](#)]
24. Cano, E.; Lafuente, D.; Bastidas, D.M. Use of EIS for the evaluation of the protective properties of coatings for metallic cultural heritage: A review. *J. Solid State Electrochem.* **2009**, *14*, 381–391. [[CrossRef](#)]
25. Xue, B.; Yu, M.; Liu, J.; Li, S.; Xiong, L.; Kong, X. Corrosion Protective Properties of Silane Functionalized Graphene Oxide Film on AA2024-T3 Aluminum Alloy. *J. Electrochem. Soc.* **2016**, *163*, C798–C806. [[CrossRef](#)]
26. Mora, L.V.; Taylor, A.; Paul, S.; Dawson, R.; Wang, C.; Taleb, W.; Owen, J.; Neville, A.; Barker, R. Impact of silica nanoparticles on the morphology and mechanical properties of sol-gel derived coatings *Surf. Coat. Technol.* **2018**, *342*, 48–56. [[CrossRef](#)]
27. Saxena, S.; Tyson, T.A.; Shukla, S.; Negusse, E.; Chen, H.; Bai, J. Investigation of structural and electronic properties of graphene oxide. *Appl. Phys. Lett.* **2011**, *99*, 013104. [[CrossRef](#)]
28. Krishnamoorthy, K.; Jeyasubramanian, K.; Premanathan, M.; Subbiah, G.; Shin, H.S.; Kim, S.J. Graphene oxide nanopaint. *Carbon* **2014**, *72*, 328–337. [[CrossRef](#)]